Vietnam Journal of Science and Technology ***63*** *(3) (2025) 528-539*

doi:10.15625/2525-2518/18501

A high effective $CuInS_2$ photocatalyst for oxidative desulfurization of dibenzothiophene in fuel oil

Nui Xuan Pham*, Thi Thanh Pham, Thuy Vi Vo Hoang, Thi Duyen Nguyen, Thanh Lam Nguyen

Department of Chemical Engineering, Hanoi University of Mining and Geology, 18 Vien Street, Duc Thang Ward, Bac Tu Liem District, Ha Noi, Viet Nam

*Email: *phamxuannui@humg.edu.vn*

Received: 10 July 2023; Accepted for publication: 27 September 2023

Abstract. In this study, $CuInS_2$ materials were synthesized by hydrothermal method. The effect of different reaction times was investigated. The structure and morphology of the materials were characterized by XRD, SEM, TEM, UV-Vis and EDX measurement methods. The obtained results showed that with a reation time of 24 h, the $CuInS_2$ sample (CIS-24) had an average particle size of about 50 nm and a band gap energy value of E_g = 1.48 eV, with the ability to strongly absorb visible light. The photocatalytic activity of CIS-24 was investigated by the degradation of dibenzothiophene under visible light irradiation. The photocatalytic efficiency reached a maximum of 97.9 % at an initial concentration of 500 ppm after 5 h of reaction at 70 ^oC with a catalyst dosage of 50 mg and 1.0 mL of H_2O_2 as an oxidant.

Keywords: $CuInS_2$, oxidative desulfurization, photocatalyst, dibenzothiophene, diesel fuel.

Classification numbers: 3.3.3, 3.4.2, 3.7.3

1. INTRODUCTION

As is well known, the presence of sulfur-containing organic compounds in liquid hydrocarbon fuels is a cause of air pollution and acid rain due to the release of sulfur oxides (SO_x) during fuel combustion. Many countries have established regulations requiring a maximum sulfur content of 10 ppm in gasoline to ensure environmental standards beginning in 2017. Therefore, the deep desulfurization technology in fuel has been receiving research attention [1 - 5]. Due to the use of hydrodesulfurization (HDS) technology in petrochemical refineries, a high temperature of 300 - 400 ^oC and 100 atm of pressure are required, and a large amount of hydrogen gas is required to separate heterocyclic compounds such as thiophene, benzothiophene (BT), dibenzothiophene (DBT), especially 4,6 alkyl DBT, etc. Due to the presence of aromatic rings in the molecules, these compounds are difficult to remove, thus enhancing the aromatic properties [6]. In addition, many methods have been studied, such as biological desulfurization (BDS) [7], adsorbent desulfurization (ADS) [8] to achieve deep desulfurization with limited threshold. Sulfur concentrations in diesel fuel are expected to be regulated at 5 ppm weight (ppmw). Among these methods, oxidative desulfurization (ODS)

technology is one of the effective methods that complement HDS. This technology uses an oxidizing agent for the oxidation of sulfur-containing organic compounds to a strong polarizer and the product is separated by adsorption or extraction. ODS technology operates under mild conditions (atmospheric pressure and temperature below 100 ^oC) with high selectivity [9, 11]. Therefore, ODS technology is considered a promising sulfur separation technology with high efficiency and low production cost.

Furthermore, photocatalytic oxidation of sulfur-containing compounds in fuels has been studied by scientists. Recently, Pham *et al*. [12, 13] reported the use of Ag@AgBr/Al-SBA-15 green catalyst and Ti-containing Al-SBA-15 mesostructured catalysts for the photocatalytic oxidation of DBT under sunlight irradiation. Feng *et al*. [14] have shown that photocatalytic oxidation is effective to remove sulfur-containing organic compounds in fuel oil and pollutants such as rhodamine B (RhB) present in wastewater by using Pt-RuO_2/TiO_2 photocatalysts. Aazam *et al*. [15] studied the photocatalysis of cyanide oxidation under visible light by Pt phase $AgInS_2$ nanoparticles. Among the various photocatalysts, metal sulfides such as $ZnIn_2S_4$, $MInS_2$ (M: Ag, Cu) are the most common photocatalysts and have been used for hydrogen energy development because of its non-toxicity, high stability and ability to absorb visible light over a wide range [16 - 19].

$CuInS_2$ materials are known to be typical p-type catalysts with potential for hydrogen separation from water, photocatalysis for CO_2 reduction, and treating organic pollutants [20 - 25]. Along with that, the high absorption efficiency (~10^5 cm^{-1}) [1] and the near-optimal bandgap energy (~1.53 eV) allow to fully absorb the energy of sunlight with wavelength greater than 800 nm and obtain high absorption efficiency per unit length. Besides, sulfur-containing organic compounds such as BT, DBT and DBT derivatives are catalyzed by photocatalysts combined with visible light irradiation where they are oxidized to sulfone or sulfide compounds. These compounds are separated from fuel by adsorption or extraction methods. Thus, $CuInS_2$ material acts as an effective photocatalyst in the oxidative desulfurization of DBT in fuel.

In this paper, ternary sulfide semiconductors of CIS were synthesized for use as photocatalysts and demonstrated their excellent photocatalytic performance in the degradation of DBT.

2. EXPERIMENTAL

2.1. Materials

All chemicals, including sodium dodecyl sulfate ($C_{12}H_{25}NaO_4S$, 99.1 %), dibenzothiophene (DBT, 99.0 %), indium chloride ($InCl_3$, 98 %), *n*-octane (C_8H_{18}, 99.0 %), thioacetamide (C_2H_5NS, 99.0 %), ethylene glycol ($C_2H_6O_2$, 99.0 %), cupper(I) iodide (CuI, 99.2 %), ethanol (C_2H_5OH, 99.0 %) and hydroperoxide (H_2O_2, 30 %), were purchased from Sigma-Aldrich. Deionized water (DI) was used in all synthesis processes.

2.2. Synthesis of $CuInS_2$ photocatalyst

$CuInS_2$ material was synthesized by a simple hydrothermal method, specifically as follows: 2.8838 g of sodium dodecyl sulfate (SDS) was dissolved in 50 mL of ethylene glycol and heated at 70 ^oC for 15 min. Next, the above solution was added with 0.39 g of CuI, 0.44236 g of $InCl_3$, 0.7513 g of thioactemide and continued to be heated for 30 min to homogenize the solution. Then, the solution was put into a hydrothermal Teflon flask at 180 ^oC for different times of 9, 12

and 24 h. The obtained solid with a black color was washed thoroughly with deionized water and ethanol at 60 °C for 3 h. Finally, the catalytic samples were obtained after drying at 80 °C for 5 h, and the samples were designated by time, namely CIS-9, CIS-12 and CIS-24.

2.3. Characterization

The X-ray diffraction pattern was recorded on a D8–Advance Bruker instrument with CuKα emission (wavelength λ = 1.54 Å), power 40 kV, 40 mA. The morphology was determined on a Hitachi S4800 (Japan) scanning electron microscope (SEM) and CIS nanoparticles were then examined by transmission electron microscopy (TEM, Leica IEO 906E). Diffuse reflectance spectroscopy (DRS) was obtained with a Shimadzu-UV–2550–8030 spectrometer in the range of 190 - 800 nm with a slit width of 5.0 nm and a light source with a wavelength of 360 nm at low temperature (room level). In addition, energy X-ray spectroscopy (EDX) was used to determine the composition of the material.

2.4. Photocatalytic activity test

In DBT photocatalytic oxidation experiments, visible light was used as the energy source. The "model" fuel sample containing DBT (500 ppm) was mixed with 0.2875 g of DBT in 100 mL of *n*-octane solvent. In experimental batches, 50 mL of DBT and 50 mg of CIS photocatalyst were placed in a three-necked flask immersed in water and stirred on a magnetic stirrer at 500 rpm. Before the photocatalytic oxidation process started under visible light irradiation, the mixture was placed in the dark for 30 min to reach adsorption-desorption equilibrium. The suspension was then irradiated under a 50 W light-emitting diode (LED) lamp with the wavelengths ranging from 400 to 700 nm, corresponding to a visible light region. The experiments were surveyed according to the parameters of temperature and oxidant content over time. The degradation of DBT was determined based on the absorbance at λ_{max} = 325 nm using a UV–Vis spectrophotometer. The degradation efficiency was calculated as follows:

$$\eta = \frac{C_o - C_t}{C_o} \times 100\% \quad (1)$$

where C_o represents the initial DBT concentration and C_t represents the residual DBT concentration at each irradiation interval.

3. RESULTS AND DISCUSSION

3.1. Characterization of samples

X-ray diffraction (XRD) pattern of CIS nanoparticles at different reaction times is shown in Figure 1. All of the main reflection peaks of CIS at 2θ of 27.4°, 31.6°, 44.8°, and 55.4° are assigned to the (112), (004), (204)/(220), and (116)/(312) crystal planes of chalcopyrite-type CIS (JCPDS card No. 38-0777), respectively [26]. The sample is indexed as a tetragonal phase which is very close to the values in the literature (JCPDS No. 38-0777). After being proceeded for 6, 12 h, besides the diffraction peak of a tetragonal CIS structure phase, the existence of a hexagonal CuS structure is found (JCPDS card No. 01–1281). However, the diffraction peak intensity of the CIS phase becomes gradually stronger as the reaction time increases up to 24 h while that of the CuS phase completely disappears, which indicates the improved purity and crystallinity of the CIS crystals, that is, after the reaction time was prolonged to 24 h, pure CIS with high crystallinity was obtained. Thus, the CIS-24 was used for further study.

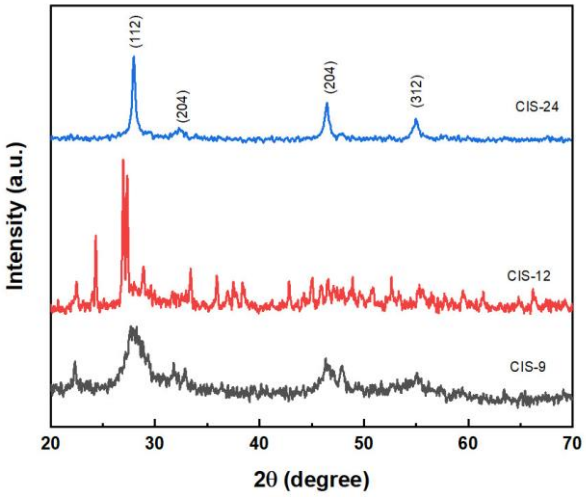

Figure 1. XRD diffraction patterns of CIS synthesized at 180 ^{o}C with different reation times.

The morphology of CIS-24 was investigated using SEM images in Figure 2, showing coral-like microstructures composed of nano-rods [27]. To further investigate the morphological details, TEM images of the sample is shown in Figure 3, demonstrating that the CIS sample consists of nanoparticles with spherical microstructure forming homogeneous blocks. The average size of the particles is about 50 nm.

Additionally, the FT–IR spectrum of the CIS-24 sample is shown in Figure 4a. The absorption bands between 1651 and 1556 cm^{-1} correspond to the stretching vibrations of the S–In and S–Cu bonds [28]. Besides, two other very weak peaks at about 2985 and 2883 cm^{-1} correspond to the stretching vibration of the sp^3C–H absorption. This may be due to traces of SDS used during the synthesis of CIS. A new band located at 1062 cm^{-1} attributes to the stretching vibration of the S–O bond which could be formed through the reaction of unsaturated S vacancies in CIS and O atoms in physically adsorbed water.

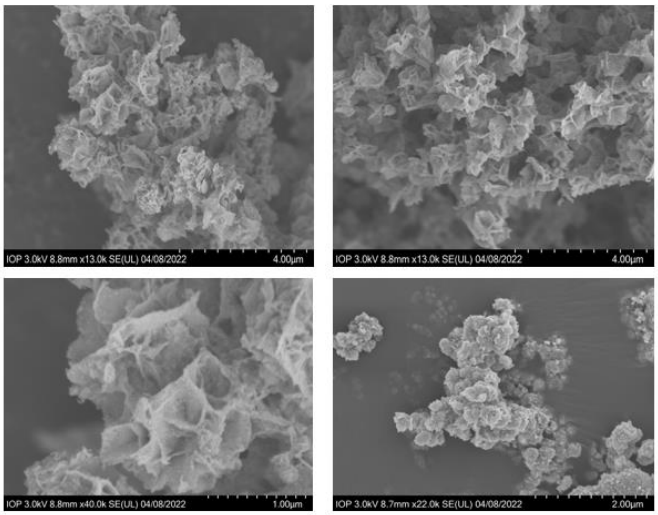

Figure 2. SEM images of the synthesized CIS-24 sample.

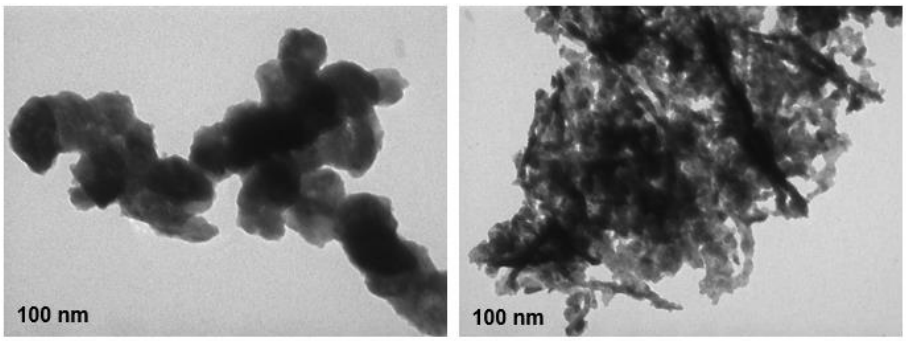

Figure 3. TEM images of the synthesized CIS-24 sample.

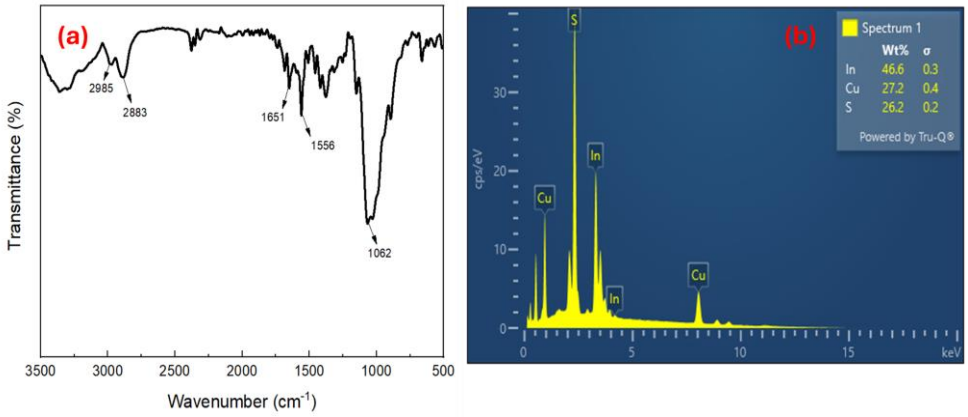

Figure 4. (a) FT-IR spectrum, and (b) EDX spectrum of the synthesized CIS-24 sample.

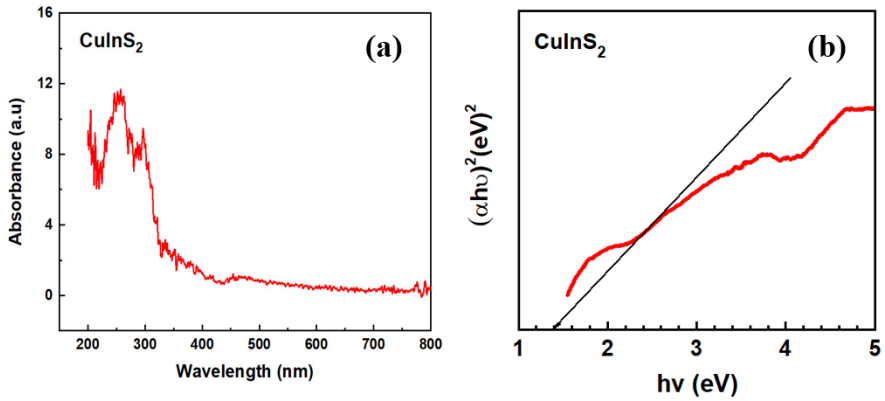

Figure 5. (a) Diffuse reflectance spectrum, and (b) bandgap energy of the CIS-24 sample.

To detect the coexistence of the elements present and their molar proportions, EDX analysis of the CIS sample was carried out. As shown in Figure 4b, the Cu, In and S species were all detected in the $CuInS_2$ sample and the molar ratio of Cu to In and S was close to 1:1:2 as a percentage of atoms which is consistent with the stoichiometry of $CuInS_2$ [29].

UV-Vis diffuse reflectance spectroscopy was also used to confirm the optical properties of the material. It can be seen that CIS-24 exhibits absorption in the visible light range (λ = 200 -

500 nm) (Figure 5a). The bandgap energy of the sample can be calculated by the plot of transformed Kubelka–Munk functions, and the bandgap energy of the photocatalyst is obtained using Eq. (2).

$$\alpha hv = A(hv - E_g)^{n/2} \quad (2)$$

where α, v, E_g, and A are the absorption coefficient, light frequency, bandgap, and a constant representing the proportion of reflected light, respectively.

Following the linear line passing through the inflection point of the horizontal shear curve (Figure 5b) gives the bandgap energy value of CIS-24 as E_g = 1.48 eV, consistent with the reported value [30]. This result demonstrates the strong visible light absorption ability of the material and the potential use of CIS as a photocatalyst operating under visible light irradiation.

3.2. Photodegradation of DBT under sunlight irradiation

The photocatalytic activity of CIS-24 was investigated for the degradation of DBT under visible light irradiation at different temperatures of 50 °C, 60 °C and 70 °C with 50 mL of DBT (250 ppm DBT in *n*-octane), 1 mL of H_2O_2 and 50 mg of photocatalyst (Figure 6a). The results showed that in the dark, at all three temperatures above, the photocatalytic reaction did not occur and the adsorption capacity of DBT increased from 16.3 % to 22.35 % when the temperature increased from 50 °C to 70 °C, respectively.

The results obtained after visible light irradiation and using H_2O_2 as oxidizing agent showed that the conversion of DBT increased with temperature (Figure 6b). Specifically, the conversion reached 73.89 %, 75.6 % and 92.33 % at reaction temperatures of 50 °C, 60 °C and 70 °C, respectively, within 5 h. Thus, at a higher temperature (70 °C) the rate of free radical generation increased, leading to an increase in DBT conversion.

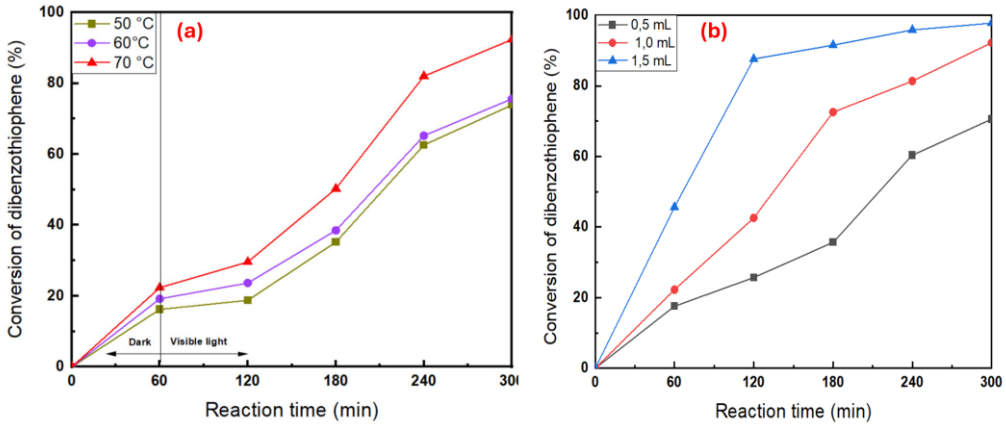

Figure 6. DBT conversion on CIS-24 catalyst (a) at different temperatures (Reaction conditions: V_{DBT} = 50 mL, V_{H2O2} = 1.0 mL, $m_{catalyst}$ = 50 mg), and (b) with different amounts of H_2O_2 oxidizing agent under visible light irradiation (Reaction conditions: V_{DBT} = 50 mL, T = 70 °C, $m_{catalyst}$ = 50 mg).

The amount of oxidizing agent H_2O_2 has a significant effect on the conversion of DBT in the photocatalytic reaction. With 0.5 mL of H_2O_2, the conversion reached only 69.5 %. However, with an increase in the amount of H_2O_2 from 1.0 to 1.5 mL, the efficiency of DBT conversion increased significantly from 92.33 % to 97.9 % after 5 h. As is known, H_2O_2 is a strong oxidizing agent and produces hydroxyl radicals when exposed to light. When low concentrations of H_2O_2 (< 0.5 mL) are used, the reaction between hydroxyl radicals and H_2O_2

occurs, the $^{\cdot}OH$ radicals needed to facilitate the oxidation reaction become more difficult. Therefore, the sulfur removal efficiency is lower when using a small amount of oxidizing agent.

Because of narrow bandgap of CIS (E_g = 1.48 eV), it can be excited by visible light. The surface of the CIS photocatalyst is irradiated by this light, generating electrons ($\bar{e}$) and holes (h^+). The photogenerated electrons on the conduction band (CB) of CIS transfer to the valence band (VB). In the next step, the excited electrons on CB are captured by oxygen molecules adsorbed on the surface, generating superoxide anions:

$$(O_2^{\cdot -}): O_2 + \bar{e} \rightarrow O_2^{\cdot -} \quad (3)$$

Also, the presence of h^+on the CIS surface leads to the formation of hydroxyl radicals ($HO^{\cdot}$):

$$H_2O + h^+ \rightarrow {}^{\cdot}OH \quad (4)$$

These species oxidize DBT adsorbed on the catalyst surface. The possible mechanism for the photocatalytic oxidation of DBT is as follows [31, 32]:

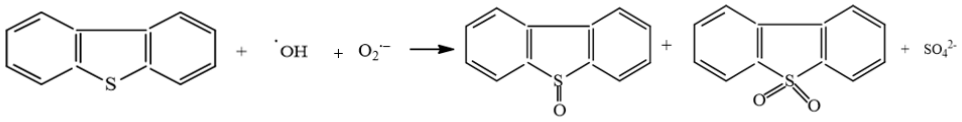

Scheme 1. Schematic diagram of the photocatalytic oxidation of DBT.

3.3. Kinetics of photocatalytic degradation

From the above-mentioned experiments, all the optimal reaction conditions were used in the catalytic degradation. The optimum conditions were 1.5 mL H_2O_2, 50 mL DBT (250 ppm DBT in *n*-octane) and 50 mg catalyst with reaction temperatures of 50 ^oC, 60 ^oC and 70 ^oC. The photocatalytic degradation of DBT as a function of irradiation time in the presence of the CIS-24 catalyst can be described by a first-order reaction, as shown in expression (5):

$$-\ln\left(\frac{C_t}{C_o}\right) = k_p t \quad (5)$$

where C_t and C_o are concentrations at time t and initial time, respectively, k_p is the first order reaction rate constant and t is the irradiation time (h). The equation shown in Figure 7 is analyzed by first-order kinetics and the rate constant can be deduced from expression (3).

The first-order kinetics of the desulfurization reaction with the CIS-24 catalyst is determined at different temperatures (Figure 9). Specifically, y = 0.123x + 0.003 with correlation coefficient R^2 = 0.9871, y = 0.0624x + 0.1037 with R^2 = 0.9808, y = 0.0044x + 0.007 with R^2 = 0.9856 at temperatures of 70 ^oC, 60 ^oC, 50 ^oC, respectively. All linear graphs are consistent with first-order reaction (R^2 > 0.98). The rate constants (k_p) at 70 ^oC, 60 ^oC, and 50 ^oC were measured to be 0.7923, 0.4565 and 0.256 h^{-1}, respectively. The half-life of the experiment was calculated by replacing C_t with C_o/2.

$$t_{1/2} = \frac{0.693}{k_p} \quad (6)$$

where $t_{1/2}$ is the half-life (h).

According to the kinetic study, the half-life ($t_{1/2}$) for the DBT degradation reactions was determined to be 0.78, 1.51 and 2.7 h at reaction temperatures of 70 ^{o}C, 60 ^{o}C, 50 ^{o}C, respectively. These results indicate that the relatively fast degradation rate of DBT increases with increasing reaction temperature up to 70 °C, which is consistent with the increase in reaction temperature and reaction rate according to the Arrhenius equation, resulting in higher DBT conversion [31].

Therefore, the photocatalytic oxidative degradation of DBT in *n*-octane solvent using 50 mg of CIS-24 was a pseudo-first-order reaction.

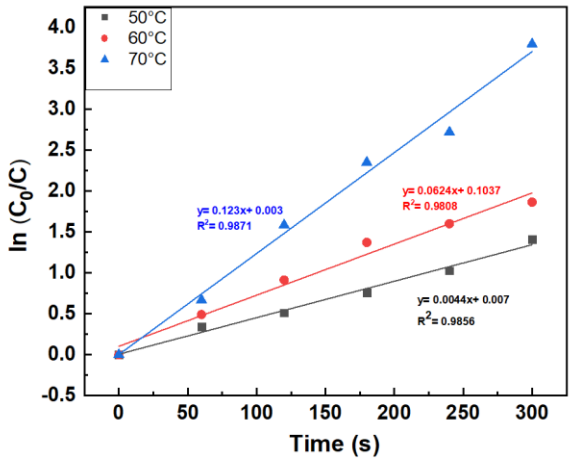

Figure 7. Pseudo-first-order kinetic model for DBT degradation by photocatalytic oxidative desulfurization at different temperatures.

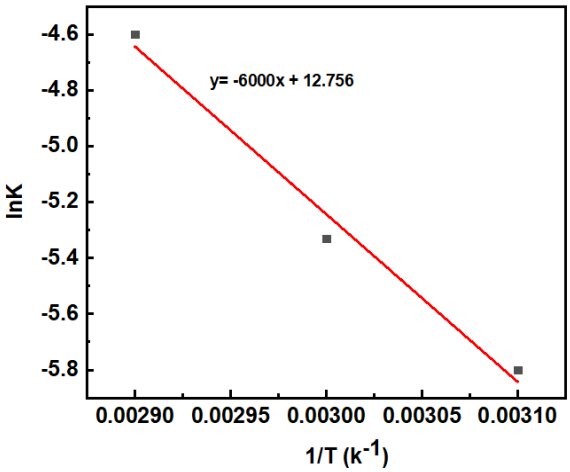

Figure 8. Arrhenius plot for the photocatalytic degradation of DBT.

The dependence of the rate constant *k* on the temperature response is expressed by the Arrhenius equation:

$$k=A.e^{-\frac{E_a}{RT}} \quad (7)$$

Accordingly,

$$\ln k = -\frac{E_a}{R}\frac{1}{T} + \ln A \quad (8)$$

where E_a is the activation energy, A is the pre-exponential constant , R is the gas constant, and T is the reaction temperature (K). The Arrhenius diagram for a first-order reaction is shown in Figure 8. The apparent activation energy (E_a) was calculated from the slope and intercept of the Arrhenius plot, giving a value of 48.22 kJ/mol. This value is similar to the result of the oxidation of DBT in H_2O_2/acetic acid using polyoxometalate as a catalyst. Lorena *et al*. [33] applied first-order rate constants to the oxidation of DBT at different temperatures and obtained an E_a value of 43.4 kJ/mol.

4. CONCLUSIONS

In conclusion, a multi-metallic sulfide material of CIS was successfully synthesized by a simple hydrothermal method using thioacetamine, CuI and $InCl_3$. CIS nanoparticles were formed with an average particle size of 50 nm and a low band gap energy E_g = 1.48 eV. The results of photocatalytic degradation of DBT using CIS catalyst showed that the sulfur removal efficiency reached 97.76 % with an initial concentration of 500 ppm after 5 h at a reaction temperature of 70 ^oC, using 1.5 mL of H_2O_2 and 50 mg of catalyst under visible light irradiation. The photocatalytic oxidative degradation of DBT using CIS-24 followed pseudo-first-order kinetics and the activation energy was 48.22 kJ/mol.

Acknowledgments. This research was funded by the Young Talent Fund for Students of Hanoi University of Mining and Geology.

CRediT authorship contribution statement. Pham Xuan Nui: Methodology, Conceptualization, Review and Editing. Pham Thi Thanh: Investigation, Data analysis, Writing original draft. Vo Hoang Thuy Vi: Formal analysis. Nguyen Thi Duyen: Data curation. Nguyen Thanh Lam: Investigation.

Declaration of competing interest. The authors declare that they have no known competing financial interests or personal relationships that could have appeared to influence the work reported in this paper.

REFERENCES

1. Saiyasitpanich P., Lu M., Keener T. C., Liang F., Khang S. J. - The effect of diesel fuel sulfur content on particulate matter emissions for a nonroad diesel generator, J. Air Waste Manage Assoc. **55** (2005) 993-998. doi: 10.1080/10473289.2005.10464685.
2. Shah S. D., Cocker D. R., Miller J. W., Norbeck J. M. - Emission rates of particulate matter and elemental and organic carbon from in-use diesel engines, Environ. Sci. Technol. **38** (2004) 2544-2550. doi: 10.1021/es0350583.
3. Maricq M. M., Chase R. E., Xu N., Laing P. M. - The effects of the catalytic converter and fuel sulfur level on motor vehicle particulate matter emissions: Light duty diesel vehicles, Environ Sci Technol. **36** (2002) 283-289, doi: 10.1021/es010961t.
4. Zielinska B., Sagebiel J., McDonald J. D., Whitney K., Lawson D. R. - Emission rates and comparative chemical composition from selected in-use diesel and gasoline-fueled vehicles, J. Air Waste Manage. Assoc. **54** (2004) 1138-1150. doi:10.1080/ 10473289.2004.10470973.
5. Ge L., Liu Q., Hao N., Kun W. - Recent developments of photoelectrochemical biosensors for food analysis, J. Mater. Chem. B **7** (2019) 7283-7300. doi: 10.1039/C9TB01644A.

6. Houalla M., Broderick D. H., Sapre A. V., Nag N. K., de Beer V. H. J., Gates B. C., Kwart H. - Hydrodesulfurization of methyl-substituted dibenzothiophenes catalyzed by Co-Mo/gamma-Al_2O_3, J. Catal. **61** (1980) 521-523. doi: 10.1016/0021-9517(80)90400-5.
7. Guchhait S., Biswas D., Bhattacharya P., Chowdhury R. - Bio-desulfurization of model organo-sulfur compounds and hydrotreated diesel–experiments and modeling, Chem. Eng. J. **112** (2005) 145-151. doi: 10.1016/j.cej.2005.05.006.
8. Shen Y., Li P., Xu X., Liu H. - Selective adsorption for removing sulfur: a potential ultra-deep desulfurization approach of jet fuels, RSC Adv. **2** (2012) 1700-1711, doi: 10.1039/C1RA00944C.
9. Ma X., Zhou A., Song C. - A novel method for oxidative desulfurization of liquid hydrocarbon fuels based on catalytic oxidation using molecular oxygen coupled with selective adsorption, Catal. Today **123** (2007) 276-284. doi: 10.1016/j.cattod.2007.02.036.
10. Zhao D., Wang J., Zhou E. - Oxidative desulfurization of diesel fuel using a Brønsted acid room temperature ionic liquid in the presence of H_2O_2, Green Chemistry **9** (2007) 1219-1222. doi: 10.1039/B706574D.
11. Lü H., Gao J., Jiang Z., Yang Y., Song B., Li C. - Oxidative desulfurization of dibenzothiophene with molecular oxygen using emulsion catalysis, Chem. Comm **2** (2007) 150-152. doi: 10.1080/10916460903030441.
12. Pham X. N., Nguyen M. B., Ngo H. S., Doan H. V. - Highly efficient photocatalytic oxidative desulfurization of dibenzothiophene with sunlight irradiation using green catalyst of Ag@AgBr/Al-SBA-15 derived from natural halloysite. J. Ind. Eng. Chem. **90** (2020) 358-370. doi: 10.1016/j.jiec.2020.07.037.
13. Pham X. N., Nguyen M. B., Doan H. V. - Direct synthesis of highly ordered Ti-containing Al-SBA-15 mesostructured catalysts from natural halloysite and its photocatalyticactivity for oxidative desulfurization of dibenzothiophene. Adv. Powder Tech. **31** (2020) 3351-3360. doi: 10.1016/j.apt.2020.06.028.
14. Feng L., Yongna Z., Lu W., Yuliang Z., Donge W., Min Y., Jinhui Y., Boyu Z. and Zongxuan J. and Can L.- Highly efficient photocatalytic oxidation of sulfur-containing organic compounds and dyes on TiO_2 with dual cocatalysts Pt and RuO_2, Appl. Catal. B **127** (2012) 363-370. doi: 10.1016/j.apcatb.2012.08.024.
15. Aazam E. S. - Photocatalytic oxidation of cyanide under visible light by Pt doped $AgInS_2$ nanoparticles, J. Ind. Eng. Chem. **20** (2014) 4008-4013. doi: 10.1016/j.jiec.2013.12.104.
16. Liang Q., Zhang C., Xu S., Zhou M., Li Z. - Nanocomposites based on 3D honeycomb-like carbon nitride with Cd0.5Zn0.5S quantum dots for efficient photocatalytic hydrogen evolution, Int. J. Hydrogen Energy **44** (2019) 29964-29974. doi:10.1016/ j.ijhydene.2019.09.180.
17. Boon-Junn N., Putri L. K., Kong X. Y., Pasbakhsh P., Chai S. P. - Overall pure water splitting using one-dimensional P-doped twinned Zn0.5Cd0.5S1-x nanorods via synergetic combination of long-range ordered homojunctions and interstitial S vacancies with prolonged carrier lifetime, Appl. Catal. B **262** (2020) 118309. doi:10.1016/ j.apcatb.2019.118309.
18. Haifeng L., Bowen S., Hui W., Qinqin R., Yanling G., Yanyan L., Jiakun W., Wenjing W., Jie L., Xun W. - Unique 1D $Cd_{1-x}Zn_xS$@O-MoS_2/NiO_x nanohybrids: Highly efficient

visible-light-driven photocatalytic hydrogen evolution via integrated structural regulation, Small **15** (2019) 1804115. doi: 10.1002/smll.201804115.

19. Choi Y., Beak M., Yong K. - Solar-driven hydrogen evolution using a $CuInS_2$/CdS/ZnO heterostructure nanowire array as an efficient photoanode, Nanoscale **6** (2014) 8914-8918, doi:10.1039/c4nr01632g.
20. Jing H., Mélina G. G., Bo X., Palas B. P., Ahmed S. E., Lei T., Junliang S., Leif H., Haining T. - Covalently linking $CuInS_2$ quantum dots with a Re catalyst by click reaction for photocatalytic CO_2 reduction, Dalton Trans. **47** (2018) 10775-10783. doi:10.1039/c8dt01631c.
21. Sandroni M., Gueret R., Wegner K. D., Reiss P., Fortage J., Aldakov D., Collomb M.-N. - Cadmium-free $CuInS_2$/ZnS quantum dots as efficient and robust photosensitizers in combination with a molecular catalyst for visible light-driven H_2 production in water, Energy Environ. Sci. **11** (2018) 1752-1761. doi: 10.1039/C8EE00120K.
22. Yong-Jun Y., Da-Qin C., Yan-Wei H., Zhen-Tao Y., Jia-Song Z., Ting-Ting C., Wen-Guang T., Zhong-Jie G., Da-Peng C., Zhi-Gang Z. - MoS_2 nanosheet-modified $CuInS_2$ photocatalyst for visible-light-driven hydrogen production from water, Chem. Sus. Chem. **9** (2016) 1003-1009. doi:10.1002/cssc.201600006.
23. Sheng L., Jun K., Mengqian Y., Qi Z., Peng X., Lidan D., Shaobin W. - $CuInS_2$ quantum dots embedded in Bi_2WO_6 nanoflowers for enhanced visible light photocatalytic removal of contaminants, Appl. Catal. B **221** (2018) 215-222, doi: 10.1016/j.apcatb.2017.09.028.
24. Liu L., Li H., Liu Z., Xie Y. H. - The conversion of $CuInS_2$/ZnS core/shell structure from type I to quasi-type II and the shell thickness-dependent solar cell performance, J. Colloid Interface Sci. **546** (2019) 276-284. doi:10.1016/j.jcis.2019.03.075.
25. Ilaiyaraja P., Das T. K., Mocherla P. S. V., Sudakar C. - Optical whispering gallery-enabled enhanced photovoltaic efficiency of CdS–$CuInS_2$ thin film-sensitized whisperonic solar cells, J. Phys. Chem. C **123** (2019) 1579-1586. doi: 10.1021/acs.jpcc.8b09292.
26. Thuy N. T. M., Chi T. T. K., Thuy U. T. D., Liem N. Q. - Low-cost and large-scale synthesis of $CuInS_2$ and $CuInS_2$/ZnS quantum dots in diesel, Opt. Mater. **37** (2014) 823-827. doi:10.1016/j.optmat.2014.09.016.
27. Hosseinpour-Mashkani S. M., Salavati-Niasari M., Mohandes F. - $CuInS_2$ nanostructures: Synthesis, characterization, formation mechanism and solar cell applications, J. Ind. Eng. Chem. **20** (2014) 3800-3807. doi:10.1016/j.jiec.2013.12.082.
28. Xiaofei F., Junwu T., Zizhou Z., Siwen S., Lin Z., Zuming H., Yong G., Yongmei X. - Interfacial S–O bonds specifically boost Z-scheme charge separation in a $CuInS_2$/In_2O_3heterojunction for efficient photocatalytic activity, RSC Adv. **13** (2023) 8227-8237. doi:10.1039/d3ra00043e.
29. Mousavi-Kamazani M., Salavati-Niasari M., Emadi H. - Preparation of stochiometric $CuInS_2$ nanostructures by ultrasonic method, Micro. Nano Lett. **7** (2012) 896-900. doi:10.1049/mnl.2012.0393.
30. Nawapong C., Watcharapong P., Auttaphon C., Tawanwit L., Chamnan R., Burapat I., Athipong N., Sulawan K. - Photocatalytic activity of $CuInS_2$ nanoparticles synthesized via a simple and rapid microwave heating process, Mater. Res. Express **7** (2020) 015074. doi:10.1088/2053-1591/ab6885.

31. Xie D., He Q., Su Y., Wang T., Xu R., Hu B. - Oxidative desulfurization of dibenzothiophene catalyzed by peroxotungstate on functionalized MCM-41 materials using hydrogen peroxide as oxidant, Chinese J. Catal. **36** (2015) 1205-1213. doi:10.1016/S1872-2067(15)60897-X.
32. Zhang J., Zhao D., Yang L., Li Y. - Photocatalytic oxidation dibenzothiophene using TS-1, J. Chem. Eng. **156** (2010) 528-531. doi:10.1016/j.cej.2009.04.032.
33. Lorena P. R., Verónica A. V., Brenda C. L., María V. P., María L. M., Oscar A. A., Andrea R. B. - Sulfur elimination by oxidative desulfurization with titanium-modified SBA-16, Catal. Today **271** (2016) 102-113. doi:10.1016/j.cattod.2015.07.055.